Covalency in transition-metal oxides within all-electron dynamical mean-field theory

Kristjan Haule,* Turan Birol, and Gabriel Kotliar
Department of Physics and Astronomy, Rutgers University, Piscataway, New Jersey 08854, USA
(Received 3 October 2013; revised manuscript received 5 August 2014; published 21 August 2014)

A combination of dynamical mean field theory and density functional theory, as implemented by Haule *et al.* [Phys. Rev. B **81**, 195107 (2010)], is applied to both the early and late transition metal oxides. For a fixed value of the local Coulomb repulsion, without fine tuning, we obtain the main features of these series, such as the metallic character of $SrVO_3$ and the insulating gaps of $LaVO_3$, $LaTiO_3$, and La_2CO_4, which are in good agreement with experiment. This study highlights the importance of local physics and high energy hybridization in the screening of the Hubbard interaction and how different low energy behaviors can emerge from the unified treatment of the transition metal series.

DOI: 10.1103/PhysRevB.90.075136 PACS number(s): 71.27.+a

I. INTRODUCTION

The quantum mechanical description of electrons in solids—the band theory [1–3]—offered a straightforward account for distinctions between insulators and metals. Fermi liquid theory [4] has elucidated why interactions between 10^{23} cm^{-3} electrons in simple metals can be readily neglected, thus validating inferences of free electron models. It came as a considerable surprise in the late 1930s when crystals with incomplete d bands were found insulating [5]. The term "Mott insulator" was later coined to identify a class of solids violating the above fundamental expectations of band theory [6]. Peierls and Mott stated [5] that "a rather drastic modification of the present electron theory of metals would be necessary in order to take these facts into account" and proposed that such a modification must include Coulomb interactions between the electrons. Study of correlations in solids, which are responsible for such a dramatic increase of resistivity in Mott insulators, remains in the forefront of contemporary condensed matter physics [7,8], and it was later found in many other materials, such as d- and f-electron intermetallic compounds, as well as a number of π-electron organic conductors.

The theory became predictive with the invention of the density functional theory (DFT) [9]. Within the Kohn-Sham framework, the computation of the density of the solid is reduced to a tractable problem of noninteracting electrons moving in an effective potential. The implementation of DFT within the local density approximation (LDA) and generalized gradient approximations (GGA) in the 1970s, and the increase in computational power in the past decades, made it possible to predict materials properties *ab initio*. In weakly correlated materials the computed Kohn-Sham spectra is a reasonable description of the electronic spectra. However, materials with strong correlations, and in particular Mott insulators, are not properly treated within these approximations.

It has long been recognized that electron correlations are mostly local in space—two widely separated electrons are unlikely to be significantly correlated. Within LDA, the Kohn-Sham potential in each point of space depends solely on the density at the same point, hence LDA is local for each point in three-dimensional (3D) space. However, in solids with partially filled d bands, the correlations are very strong between two electrons on the same transition metal ion, which is beyond the scope of LDA.

In the 1990s the dynamical mean field theory (DMFT) [10–13] was developed. This theory introduces nonlocality in time, which is essential for the description of paramagnetic Mott insulators. This theory is also a local theory, but it is local to a given site rather than a point in space. DMFT successfully predicted the Mott transition in the Hubbard model [14–16], as well as many other known features of correlated systems, such as the dynamical spectral weight transfer [17], the existence of a Mott endpoint, and the value of the critical exponents at this Mott endpoint [18]. The cluster-DMFT studies [19] show that these properties are genuine to the frustrated Hubbard model.

Within DMFT, the functional that contains all local correlations is known exactly, and can be calculated by solving an appropriate quantum impurity model, but the computational cost when including many interacting degrees of freedom on a given site increases exponentially, while the hybridization with noninteracting states does not increase the computational cost significantly. At present, modern computers allow us to treat interactions exactly within a complete d shell of a transition metal ion or a complete f shell in an intermetallic compound, while the rest of the states must be treated by a mean field method. The most popular choice of such a mean field method is DFT, hence the combination of the two methods, first proposed in 1997 [20], was named LDA+DMFT [21,22]. The method became very successful as it could predict properties of an extraordinary number of correlated materials previously resisting detailed material specific predictions (for a review see [21,22]). The electronic structure and unusual physical properties of many actinides [23–25], lanthanides [26–29], 3d [30–34], 4d [35,36], and 5d [37] transition metal compounds were explained using this approach.

In the early 2000s, the LDA+DMFT method was usually referring to the dynamical mean field calculation of a lattice model, namely the Hubbard model, where the hopping parameters were derived by a so-called downfolding procedure: The bands near the Fermi level were represented in terms of a small number of Wannier states [38], and the resulting Hubbard model was solved by the DMFT method. The feedback of correlations to the electronic charge distribution, and hence the Kohn-Sham potential, was often neglected. Also, usually the minimum number of Wannier states were kept in the

*haule@physics.rutgers.edu

model, which made such model calculations conceptually simple, but less predictive, as the Coulomb repulsion for a low energy model is strongly screened by the degrees of freedom eliminated from the model, hence a material specific and model specific calculation of the interaction strength U was needed to make this method predictive. The constrained RPA [39,40] was invented for that purpose, and was quite successful when the correlations are applied in the narrow energy window.

An alternative route, which avoids construction of the low energy model, was proposed by Savrasov and Kotliar [41], in which the correction (self-energy) due to the correlations is added to the Kohn-Sham potential in a very limited region of the real space, such as the muffin-tin (MT) sphere of the correlated ion. In this approach, all degrees of freedom local to an ion are treated exactly, while the nonlocal correlations are treated in a mean field way by DFT. No valence state is eliminated from the model! Kohn-Sham potential is computed on the self-consistent electronic charge. We call this methodology the all-electron method. The early implementation of this approach, together with electronic charge self-consistency, successfully predicted the phonon spectra of elemental plutonium [24], but the impurity solvers at that time were not adequate to address many other challenging problems in correlated solids. The DFT+DMFT method has rapidly matured over the last few years, as several charge self-consistent implementations in various electronic structure codes appeared [42–47], some with integrated state of the art impurity solvers [42,47].

The most significant difference between the earlier and more modern implementations of the method is the degree of localization of the electronic orbitals, which interact with strong Coulomb interaction. In the early days, a set of Wannier orbitals spanning a narrow window around the Fermi level was typically treated by the DMFT. Since the nonlocal interactions and the nonlocal correlations are neglected in the DMFT approach, one expects that a more localized choice of orbitals leads to better results within single-site DMFT approximation. Hence newer implementations applied correlations to more localized states, and kept a larger number of itinerant states in the model. A real space projector to the spherical harmonics within a MT sphere around the correlated ion $P_R(\mathbf{r}\mathbf{r}',lml'm') = Y_{lm}(\hat{\mathbf{r}})\delta_R(r-r')Y^*_{lm}(\hat{\mathbf{r}}')$ [where $\delta_R(r-r')$ is nonzero when $r < R$ and $r' < R$] is a good example of extremely localized orbitals, which hybridizes with a large number of Kohn-Sham states, spanning a large energy window in band representation. Such a set of real-space orbitals is clearly more localized than the popular choice of maximally localized Wannier orbitals [48], which are constrained to faithfully represent some set of low energy bands.

Numerous successful predictions of this all-electron DFT+DMFT were published in the past decade nevertheless, its predictive power for transition metal oxides was questioned recently in Refs. [49,50]. Namely, using Wannier functions for oxygen-p states and transition metal d states, the authors of Refs. [49,50] concluded that fine tuning of several parameters, including the double counting and the interaction U, is needed to describe the Mott insulating state in early and late transition metal oxides. Moreover, the p-d model requires occupancy of the d orbitals to be close to unity for the Mott state, while DFT solution projected to the orbitals of their choice, predicts far larger occupancies, hence this discrepancy between DFT occupancies and the DMFT requirements lead them to suggest that the self-consistent DFT+DMFT cannot describe the Mott insulating state without fine tuning the interaction U to be in the narrow range of 6 ± 1 eV and *ad hoc* fine tuning of the double counting to reproduce the experimentally observed p-d splittings. This calls for a critical reexamination of the application of the LDA+DMFT to the $3d$ series.

Our methodology [42] was tested in numerous classes of materials, such as actinides [51–59], lanthanides [25,42,60,61], transition metal oxides [34,62,63], iron superconductors [64–67], and other transition metal compounds [37,68]. However, results for early and late transition metal oxides with our methodology are not available in literature. It is therefore important to test our methodology in this class of materials, which have mostly been studied using downfolded LDA+DMFT implementations.

II. METHOD

In this work we perform DFT+DMFT calculations for a series of early transition metal oxides: $SrVO_3$, $LaVO_3$, $LaTiO_3$, and a cuprate parent compound La_2CuO_4; all the test cases which required fine tuning in Refs. [49,50]. We show that no fine tuning or adjustable parameter is required in DFT+DMFT implementation of Ref. [42], and for a fixed value of on-site Coulomb repulsion $U = 10$ eV Mott gaps in all these compounds are in reasonable agreement with experiment.

The all-electron DFT+DMFT implementation [42] extremizes the following functional [21]:

$$\begin{aligned}\Gamma[\rho, V_{\rm KS}, G_{\rm loc}, \Sigma, V_{\rm dc}, n_d] \\ = -\mathrm{Tr}\ln\Big[(i\omega+\mu+\nabla^2-V_{\rm KS})\delta(\mathbf{r}-\mathbf{r}') \\ - \sum_{\tau LL'} P(\mathbf{r}\mathbf{r}',\tau LL')(\Sigma - V_{\rm dc})_{L'L}\Big] \\ - \int [V_{\rm KS} - V_{\rm ext}]\rho d^3r - \mathrm{Tr}\,(\Sigma G_{\rm loc}) + \mathrm{Tr}(V_{\rm dc} n_d) \\ + \Phi_H[\rho] + \Phi_{\rm xc}[\rho] + \Phi_{\rm DMFT}[G_{\rm loc}] - \Phi_{\rm dc}[n_d] \quad (1)\end{aligned}$$

of three pairs of conjugate variables. At the saddle point ρ, $V_{\rm KS}$ are the electronic charge density, the Kohn-Sham potential, $G_{\rm loc}$ and Σ are the local Green's function and DMFT self-energy, $V_{\rm dc}$ is the double-counting potential, and n_d is the occupancy of the correlated orbital. $\Phi_H[\rho]$ and $\Phi_{\rm xc}[\rho]$ are the Hartree and the exchange-correlation energy functionals, and $\Phi_{\rm DMFT}[G_{\rm loc}]$ is the sum of all skeleton diagrams constructed from $G_{\rm loc}$ and local Coulomb repulsion $\hat{U}$. This summation is carried out by the impurity solver. The local Coulomb repulsion $\hat{U}$ is parametrized with the Slater parametrization with $J_{\rm Hunds} = 0.7$ eV, and, if not otherwise stated, $U = 10$ eV. The impurity model is solved by the continuous-time quantum Monte Carlo method [69,70].

$V_{\rm ext}$ is the external potential, containing the material specific information. $P(\mathbf{r}\mathbf{r}',\tau LL')$ is the projector to the local correlated orbital at atom τ with angular momentum indices L,L'. We use projector $P^2(\mathbf{r}\mathbf{r}',\tau LL')$ introduced in Ref. [42]

with an energy window of ≈20 eV around the Fermi level. For the maximal locality of correlated states, this projector is implemented in real space and is nonzero only within the MT sphere of the correlated ion. In Sec. IV we test several different projectors, ranging from extremely localized to moderately delocalized, to understand the controversy in the literature regarding the DFT+DMFT results for the transition metal oxides. The vanadium and titanium t_{2g} states are treated dynamically, while the empty e_g states are treated by a static mean field. The copper ion with its almost full shell requires dynamic treatment of all five $3d$ orbitals.

For the double-counting correction, we used two methodologies: (a) The fully localized-limit (FLL) formula introduced in Ref. [71] is used in Sec. IV to ensure that the results are robust and that the simplification used elsewhere does not change the results appreciably from this standard prescription. (b) The method explained in Ref. [42] is used in most of this paper, where $\Phi_{\rm dc}[n_d] = n_d V_{\rm dc}$ and $V_{\rm dc}$ is also parametrized by the standard fully localized-limit formula [71] $V_{\rm dc} = U(n_d^0 - 1/2) - J/2(n_d^0 - 1)$, and n_d^0 is taken to be the nominal occupancy of the correlated ion. We name this method fixed DC. In particular, for $SrVO_3$ with the V^{4+} ion we take $n_d^0 = 1$, for $LaVO_3$ with the V^{3+} ion $n_d^0 = 2$, for $LaTiO_3$ with Ti^{3+} ion $n_d^0 = 1$, and for La_2CuO_4 with the Cu^{2+} ion $n_d^0 = 9$. This double-counting scheme has two virtues: (i) it is numerically much more stable in the charge self-consistent DFT+DMFT, as the noise from Monte Carlo does not feed back into impurity levels, and into large Hartree shifts. (ii) The results are more robust with respect to small changes in projector, linearization energies, etc. Both double countings are equally justifiable on the phenomenological level. The determination of the exact double counting is an open problem, but see recent progress in Ref. [72].

The double-counting (b) ensures that at infinite U one recovers atomic physics at the nominal valence. For discussion's sake, let us set $J_{\rm Hunds}$ to zero. In the absence of any double-counting correction, the lower Hubbard band in the atomic limit is positioned at $\varepsilon_f + U(n_d^0 - 1)$, and the upper Hubbard band at $\varepsilon_f + U n_d^0$, where ε_f is the center of the correlated state at $U = 0$ (in DFT calculation). The center between the Hubbard bands is at $\varepsilon_f + U(n_d^0 - 1/2)$. To ensure that in the large U limit the center of the correlated states does not move from its DFT position, and that we recover the correct nominal occupancy, we must subtract from the dynamic self-energy the correction $U(n_d^0 - 1/2)$, which brings the center of the correlated state to its center in DFT. Hence a good choice for the double-counting correction (in the absence of Hunds coupling) is given by $U(n_d^0 - 1/2)$, with n_d^0 as the nominal valence. In typical model calculations for the downfolded Hubbard model, such nominal valence is automatically enforced.

The DFT part of our code is based on the WIEN2k package [73]. The exchange-correlation energy in DFT ($\Phi_{\rm xc}[\rho]$) is evaluated using the PBE functional [74]. The DFT+DMFT calculations are fully self-consistent in the electronic charge density, chemical potential, and impurity levels. The temperature is set to 200 K. The experimental crystal structures from Refs. [75–78] are used for $SrVO_3$, $LaVO_3$, $LaTiO_3$, and La_2CuO_4, respectively. To obtain spectra on the real axis, maximum entropy method is used for analytical continuation of the self-energy [79]. Finally, the VESTA software is used at various points to visualize and study the crystal structures [80].

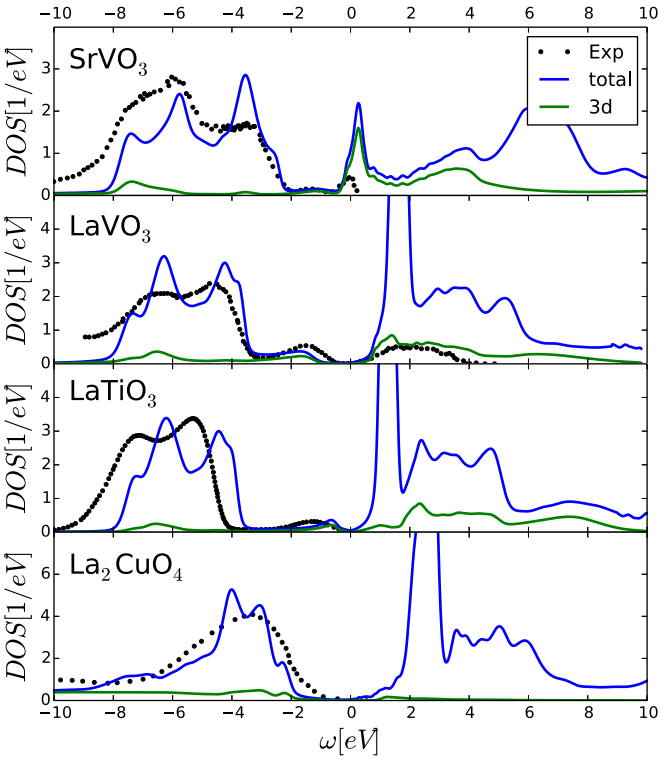

FIG. 1. (Color online) The total DOS and its projection to the $3d$ ion for selected transition metal oxides. Experimental photoemission for $SrVO_3$, $LaVO_3$, $LaTiO_3$, and La_2CuO_4 is plotted by black dots, and was digitized from Refs. [81–84], respectively.

III. RESULTS

Figure 1 shows the DFT+DMFT total and projected $3d$ densities of states for the four test compounds. The photoemission measurements are also shown for comparison. Figure 2 zooms the low energy part of the DOS to display the gap sizes. $SrVO_3$ is a mixed-valent ($n_d = 1.19$) metallic compound with oxygen states centered around -5 eV, a small shoulder corresponding to an incoherent excitation (Hubbard band) around -1.5 eV of mostly d character, and the quite broad quasiparticle peak at the Fermi level with its bandwidth reduced from DFT for roughly a factor of 2. These are all in excellent agreement with the experiment [81,85,86]. Previous LDA+DMFT calculations of Refs. [30,86], where only the t_{2g} states were treated in the model, gave very similar electronic spectra, hence results are very robust with respect to the choice of the correlated orbital. Notice that the value of U depends on the choice of energy window. Calculations with an energy window, which include only the t_{2g} states, requires a value of $U \approx 5$ eV, as used in Ref. [30]. For a large energy window (20 eV used here) a somewhat larger value of U is needed, however, results are reasonable for an extended range of U values between 6 and 10 eV.

$LaVO_3$ is a Mott insulator with a gap size of approximately 1 eV (see Fig. 2), in agreement with experiment [82]. The lower Hubbard band at -1.5 eV has a considerably more admixure

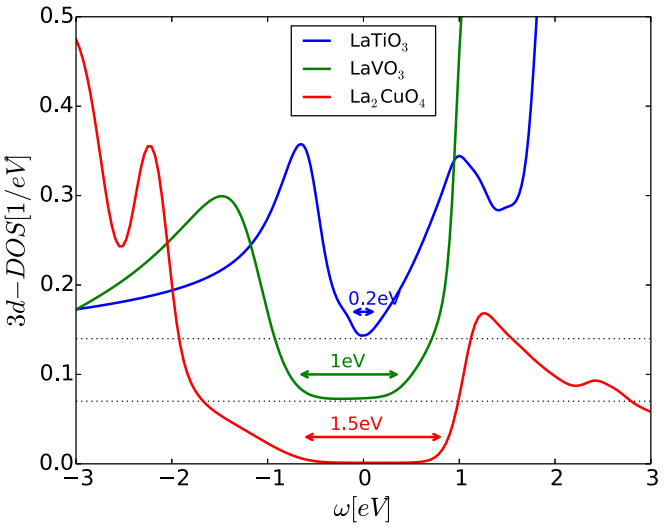

FIG. 2. (Color online) Zoom-in of the low-energy DOS projected to the $3d$ orbitals for insulating compounds. For clarity, the curves were offset for 0.07/eV. The arrows mark the experimental size of the gap.

of oxygen p than $SrVO_3$, as noticed in Ref. [82]. $LaTiO_3$ has a very small Mott gap around 0.2 eV, similar to the experimental gap [83]. The Hubbard band is located at ≈ -0.8 eV, and the oxygen-p band edge is at -4 eV. Experimentally, the Hubbard band and oxygen band are located at somewhat lower energy than theoretically predicted. Our DFT+DMFT calculation does not shift the oxygen states appreciably from its DFT position. Finally, La_2CuO_4 is a wide-gap Mott insulator of charge-transfer nature, and has a gap size of the order of 1.5 eV and the position of the oxygen-p band around -3.5 eV. The oxygen position is well predicted by the theory, and also the gap value is in good agreement with experiment [7]. Overall agreement with the experiment is very satisfactory, considering that no tuning parameter is used in these calculations.

To show that the fine tuning of local Coulomb repulsion U, which gets screened by the valence states included in our DMFT calculations, is not needed to get reasonable agreement with experiment, we show below calculations for several values of U. We also display how valence changes with the increasing correlation strength U, and, as expected, we show that an infinite U would lead to integer valence. Notice that the DFT+DMFT valence in the actinides [53] agrees with the experiment better than the LDA valence.

Figure 3 shows the dependence of DOS in $SrVO_3$ on the local Coulomb repulsion U. In the plot we also show the occupancy of the V-t_{2g} states as well as the photoemission spectra of thin film [81]. The $U = 0$ results correspond to the GGA calculation. The oxygen-p bands move to a slightly ($<$0.5 eV) lower energy at $U = 6$ eV, while they progressively move back to its DFT location at larger U. The quasiparticle peak slightly narrows with increasing U, but the Mott gap does not open even for very large U beyond 12 eV (not shown in the figure). Notice that this is inconsistent with the universal phase diagram in Fig. 2 of Ref. [50] since $n = 1.2$ falls deep inside the insulating regime for d^1 systems in that phase diagram. The lower Hubbard band, located between the quasiparticle peak and oxygen bands, appears at $U = 8$ eV and becomes

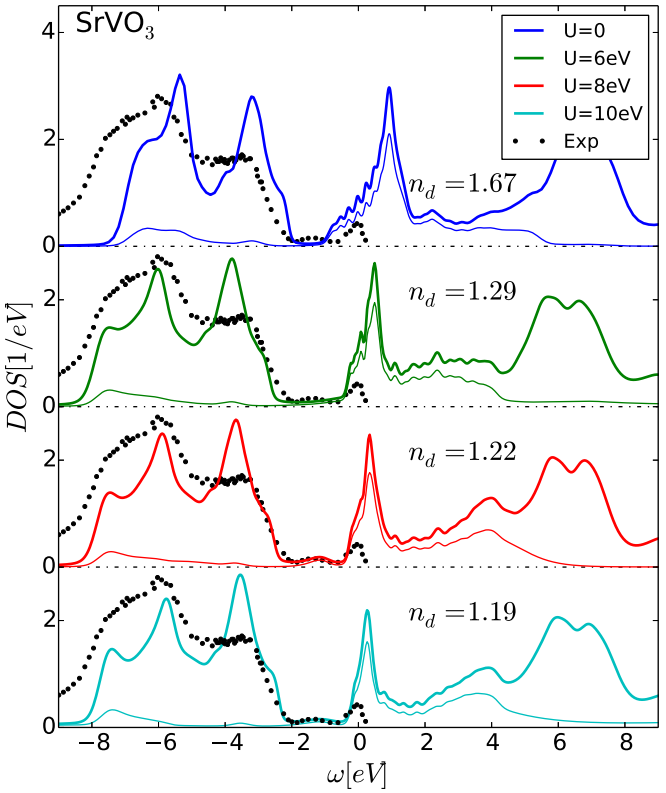

FIG. 3. (Color online) The dependence of the electronic structure of $SrVO_3$ on the value of the local Coulomb repulsion U in this all-electron calculation. The text displays the valence of the V^{4+} ion. The thick line presents the total DOS and the thin line its projection to the $3d$-ion subset. For clarity, the different electronic structures are offset for 3 eV.

even more pronounced at $U = 10$ eV. The system is very mixed valent (noninteger occupancy) in GGA, but it becomes less mixed valent with increasing U. As expected, increasing correlation strength typically reduces mixed valency. As is clear from Fig. 3, results are not very sensitive to the strength of the Coulomb repulsion, and any value of U between 6 and 12 eV gives reasonable agreement with experiment. The low energy t_{2g} spectra is in good agreement with earlier DMFT calculation of Ref. [30], which included only the t_{2g} states.

Figure 4 displays DOS for $LaVO_3$ for a range of U values. In GGA, the t_{2g} states cross the Fermi level, while the oxygen-p bands are below -3.5 eV and the La-f bands are just above the E_F. For the correlation strength of 4 eV, $LaVO_3$ is still metallic, although the quasiparticle peak becomes extremely narrow, while the valence does not change appreciably from its GGA value. Larger $U = 6$ eV opens the Mott gap (the critical U is approximately 5 eV), and an incoherent shoulder appears around -1 eV, and mixed valency is reduced. Finally, at $U = 10$ eV the Mott gap is of the order of 1 eV and the position of the incoherent shoulder is at -1.5 eV, in good agreement with experiment [82]. The partial occupancies of the t_{2g} orbitals at $U = 10$ eV are $n^1_{t2g} = 0.56$, $n^2_{t2g} = 0.76$, and $n^3_{t2g} = 0.76$, hence the orbital fluctuations are strong due to the important role of Hund's coupling, which prevents orbital polarization. This is all in good agreement with earlier DMFT calculation of Ref. [32], which considered only the low energy

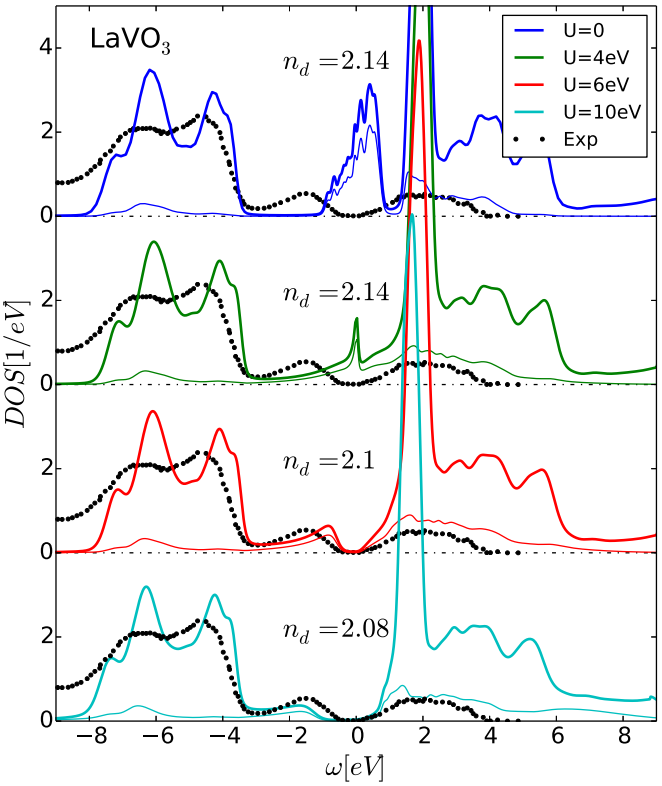

FIG. 4. (Color online) The electronic structure of $LaVO_3$ for different values of the local Coulomb repulsion U. We also display the valence of the V^{3+} ion.

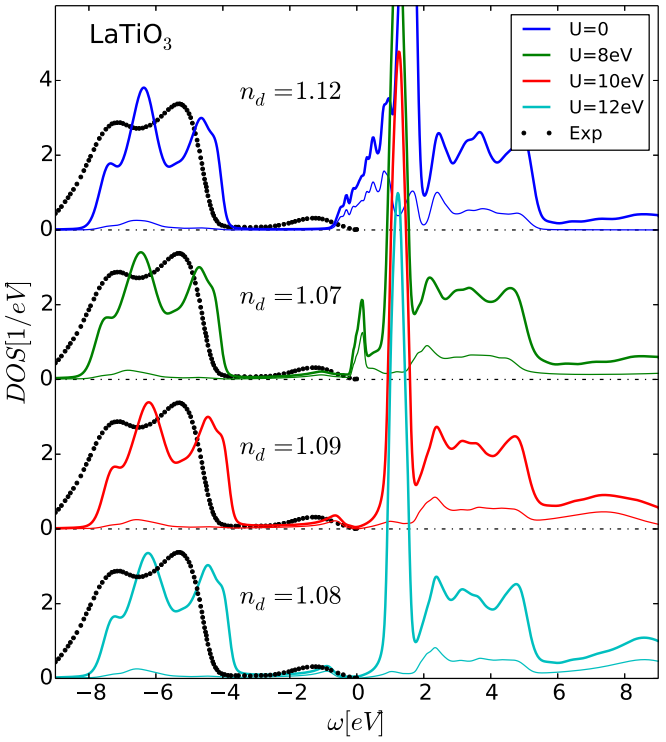

FIG. 5. (Color online) The electronic structure of $LaTiO_3$ for different values of the local Coulomb repulsion U. We also display the valence of the Ti^{3+} ion.

t_{2g} degrees of freedom. Notice that the oxygen-p bands do not shift appreciably with increasing U and their position is well determined by DFT, in strong contrast to the calculations in Ref. [49], where the oxygen-p bands move substantially for a small change in U.

In $LaTiO_3$, displayed in Fig. 5, the oxygen-p bands start around -4 eV and a very sharp La-f state appears just above the Fermi level at 1 eV. The position of this level is very sensitive to the rotation angle of the oxygen octahedra, and a larger rotation angle, which is obtained by the GGA optimization of the structure, shifts the level up by 0.5 eV compared to experimentally determined crystal structure [77] used here. This can be explained by the fact that octahedral rotations change the coordination of the A-site cation (La) drastically [87]. It is due to screening by this sharp La-f state that the Mott gap does not open for $U = 8$ eV and is very small ($\approx$0.2 eV) at $U = 10$ eV.

The orbital polarization is also very sensitive to the octahedral rotation, as pointed out in Ref. [30]. For the structure of Ref. [77], the orbital polarization is modest in our calculations ($n^1_{t2g} \approx 0.67$, $n^2_{t2g} \approx 0.20$, $n^3_{t2g} \approx 0.20$) but for only slightly larger rotation, as measured in Ref. [88], the polarization is almost complete ($n^1_{t2g} \approx 0.93$, $n^2_{t2g} \approx 0.06$, $n^3_{t2g} \approx 0.08$).

Due to the substantial hybridization of the t_{2g} states with the La-f states very near the Fermi energy (see Fig. 8), the screening is much stronger than it would be in the absence of this La-f level. Models which remove the La-f states from consideration would hence need substantially reduced interaction U to reproduce the experimentally observed Mott gap [83]. Indeed, our results clearly disagree with the phase diagram of Ref. [50], which leads us to believe that the U-n_d phase diagram is more material specific, and also depends on the presence of other states that can screen the interaction. To open a Mott gap, a near integer occupancy is needed, but the critical value of U and n_d can be quite material specific. Notice that the double counting is also proportional to the Coulomb interaction U, hence in the large U limit, the upper and lower Hubbard bands are pushed to positive and negative infinity, respectively; always resulting in an integer occupancy. We also display photoemission measurements for $La_{1-x}Sr_xTiO_{3+y}$ with $x + y = 0.04$ from Ref. [83]. The oxygen-p bands' position is somewhat different than in experiment. However, this disagreement between DFT and experiment might partially be attributed to slightly different chemical composition of the crystal. The local correlations on Ti do not improve the position of the O-p state.

Figure 6 shows the DOS for La_2CuO_4, a late transition metal oxide, and the parent compound of cuprate superconductors. Within GGA ($U = 0$), the e_g states cross the Fermi level and the t_{2g} states start at -1 eV and strongly overlap with oxygen, which starts at -2 eV. The sharp peak at 2.5 eV is due to the La-f states. The screening by La-f states in cuprates is much weaker than in $LaTiO_3$, as the hybridization function, displayed in Fig. 8, has only a very weak peak at higher energy (2.4 eV) which couples primarily to t_{2g} states, but not to a low energy $x^2 - y^2$ orbital. Once again, the oxygen-p states and the La-f states do not move appreciably with increasing correlation strength. The Mott gap opens around $U = 8$ eV. As in the model Hamiltonian studies within single site DMFT,

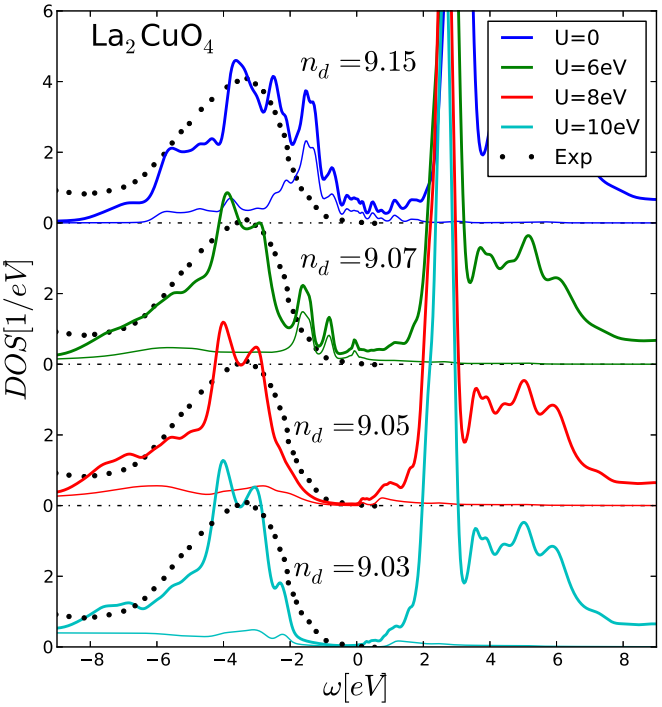

FIG. 6. (Color online) The electronic structure of La_2CuO_4 for different values of the local Coulomb repulsion U. We also display the valence of the Cu^{2+} ion.

once the insulating phase is reached [14], the gap opens discontinuously, and is of the order of 1 eV. At $U = 10$ eV, it is approximately 1.5 eV, in agreement with the experiment [7]. The oxygen bands' position is also in a good agreement with the experiment [84], centered at -3.5 eV. Figure 7 resolves DOS in orbital space. Clearly the $x^2 - y^2$ orbital is half-filled, and in the interval between -1 and -2 eV the amount of total-3d states and oxygen states is almost exactly equal. This is the region of the Zhang-Rice singlet. The z^2 orbital is sharply peaked slightly below -2 eV, and the t_{2g} states start at -3 eV.

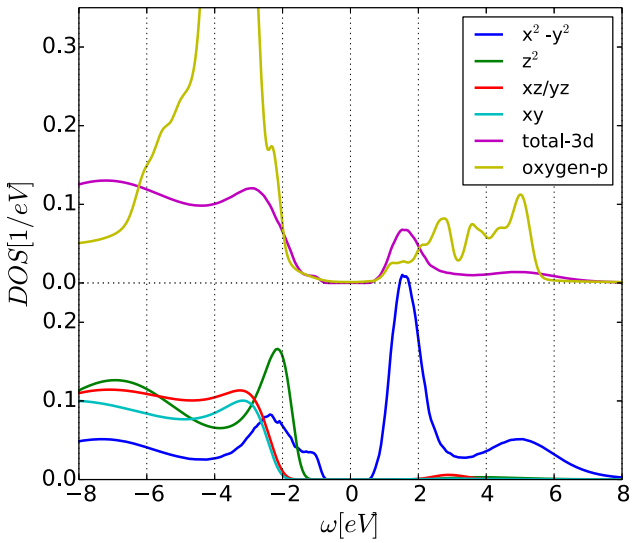

FIG. 7. (Color online) Orbitally resolved DOS for La_2CuO_4 at $U = 10$ eV. The total 3d and total oxygen-p DOS is offset for 0.25/eV.

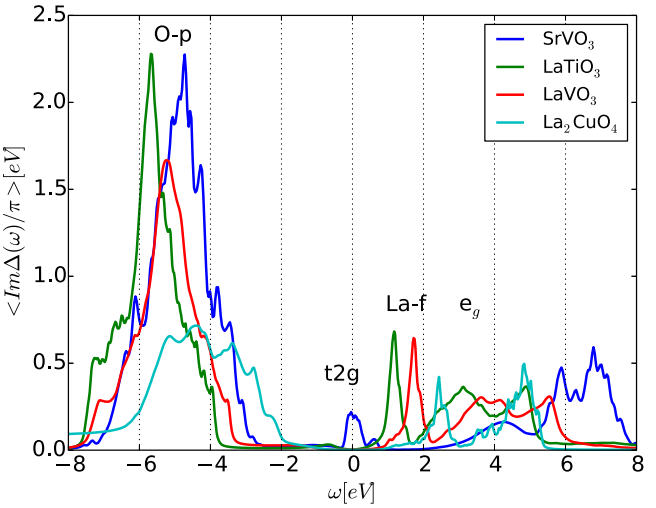

FIG. 8. (Color online) The imaginary part of the impurity hybridization function for various materials at $U = 10$ eV. We also display what is the dominant source of various peaks in the hybridization function.

A main finding of this paper is that the all-electron treatment with a large energy window requires a much larger value of U than the corresponding LDA+DMFT study with the small energy window, which keeps the t_{2g} (or e_g) states only. The bare Coulomb repulsion U of a model where all valence states are kept in the model is screened only by the degrees of freedom eliminated from the model, which are mostly core and semicore states, resulting in a much larger on-site Coulomb repulsion U in this treatment, but also more universal U across similar compounds. The screening from model U down to the fully screened interaction W is achieved here by the impurity solver (see related discussion in the context of the model in Ref. [89]).

On the one particle level, it is best demonstrated by the impurity hybridization function, which contains signatures of all the valence states in the solid that screen the local degrees of freedom. We show in Fig. 8 the average hybridization function (average over orbitals) for an electron on a transition metal site in different compounds. We can understand qualitatively the influence of the window on the characteristic scale of the impurity model from the following argument. The Kondo scale should not depend on the energy window chosen in the calculation. The Kondo scale is a function of U and impurity hybridization $T_k \approx \exp(-\text{const} \times U/\langle \text{Im}\Delta\rangle_0)$, where $\langle \text{Im}\Delta\rangle_0$ is some weighted average of the displayed hybridization function, with larger weight given to the low energy. When only the t_{2g} states in early transition metal compounds are kept in the model, U has to be small, because the hybridization function is nonzero only within the narrow region around E_F, and its average value is below 0.2 eV. When oxygen-p states are added, $\text{Im}\Delta$ increases tremendously in the interval -7 to -3 eV, and so does the weighted average $\langle \text{Im}\Delta\rangle_0$, hence U must increase to keep low energy scale intact. It is also clear from Fig. 8 that the La-f states screen the Coulomb repulsion rather well, since they are located very near the Fermi level; hence elimination of La-f states from the model would need to be compensated by a very material specific U. Finally, some extra screening is also coming from e_g states above the Fermi

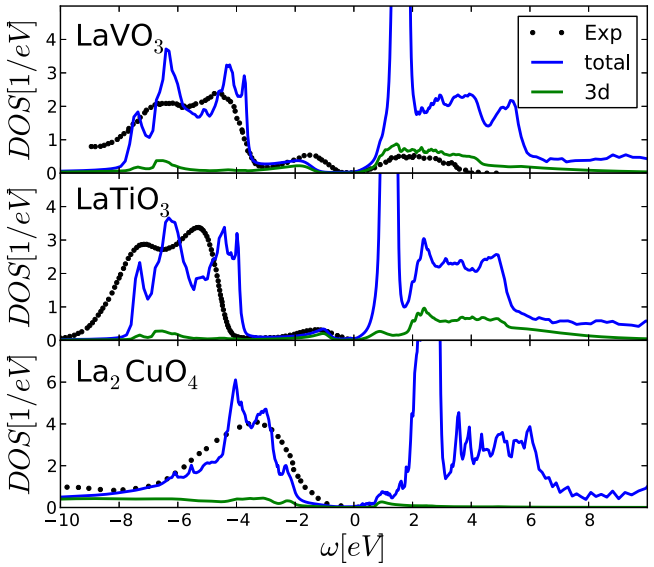

FIG. 9. (Color online) The total DOS and its projection to the $3d$ ion within DFT+DMFT for insulating transition metal oxides, computed using standard fully localized limit double counting and fixed $U = 10$ eV and $J_{\text{Hunds}} = 0.7$ eV. Experimental photoemission is the same as in Fig. 1.

level, and since their position is very material dependent, their elimination requires further tuning of U. However, when all these states are kept in the model, the large part of the screening is already contained in the model, and hence the all-electron U is rather large and more universal.

IV. DISCUSSION AND COMPARISON TO OTHER STUDIES

To asses the robustness of our results, we also tested the widely used fully localized limit (FLL) double counting of Ref. [71], namely $V_{\text{dc}} = U(n_d - 1/2) - J/2(n_d - 1)$, where n_d in the formula is computed self-consistently. We note that this makes charge self-consistency convergence a bit more challenging, but the results for the transition metal insulators studies here are almost identical to those presented above for fixed double counting.

In Fig. 9 we plot the spectral functions of all four insulators but here computed using standard FLL double counting. Comparison with Fig. 1 shows that the differences between the two double countings are extremely small and unimportant in these cases. This is not surprising given the converged DFT+DMFT occupancy of the correlated d orbitals. In Table I we list the $3d$ occupancies for the calculations presented in Fig. 1 (denominated by *fixed* DC) and for the standard FLL double counting (denominated by FLL-DC). Note that for the early transition metal oxides we count t_{2g} charge here, since correlations are applied to t_{2g} set of orbitals. For La_2CuO_4 we list total $3d$ occupancy, since the correlations are applied to all $3d$ electrons. We also tested if charge self-consistency is important for the insulating nature of these compounds. The charge self-consistent and noncharge self-consistent calculations are denoted by respectively CSS and non-CSS in Table I. The differences in occupancies are insignificant. The double counting used above (fixed DC)

TABLE I. The occupancy of the correlated $3d$ orbitals within DFT+DMFT calculation for insulating transition metal oxides. The first row is for double counting introduced in Sec. II (fixed DC) and full charge self-consistent calculation (CSC). The second row stands for fully localized limit double counting (FLL-DC) and charge self-consistency (CSS). The last column shows n_d for FLL-DC without charge self-consistency (non-CSS). R_{MT} are the muffin tin radii for the correlated atoms in atomic units.

n_d (DFT+DMFT)	Fixed DC CSC	FLL-DC CSC	FLL-DC non-CSC
La_2CuO_4 ($R_{\text{MT}} = 1.88$)	9.031	9.042	9.049
$LaVO_3$ ($R_{\text{MT}} = 1.97$)	2.075	2.098	2.093
$LaTiO_3$ ($R_{\text{MT}} = 2.01$)	1.093	1.131	1.133

makes the insulating state slightly more robust, since n_d is closest to nominal valence (of the order of 0.02 electron less than FLL-DC), the alternative FLL double counting slightly increases mixed valency, while the charge self-consistency has very small effect (of the order of 0.005) in these transition metal oxides.

In Fig. 10 we show the $3d$ DOS for La_2CuO_4 in the three types of calculations listed in Table I. There are some minor differences in the spectra distribution, and, as expected from slightly larger n_d in the FLL-DC case, the gap gets slightly smaller, but overall these differences are very small.

The above results appear to contradict conclusions of Refs. [49,50], in which the authors assert that $3d$ occupancy of LDA+DMFT calculations are consistently too large to allow the Mott insulating state. The authors then proposed to adjust the double-counting energy to allow the opening of the Mott gap within their implementation of LDA+DMFT. They traced the problem to the d occupancy being way too large even on the DFT level ($U = 0$). To define the d occupancy, they constructed the maximally localized Wannier orbitals with transition metal $3d$ and oxygen $2p$ orbitals included in the model, and excluding all the rest. In such a model they noticed that the $3d$ occupancy in La_2CuO_4 is around $n_d \approx 9.45$, in $LaVO_3$ and in $LaTiO_3$ it is around $n_{t2g} \approx 2.55$ and $n_{t2g} \approx 1.45$, respectively. These numbers are clearly larger than numbers obtained by our method at $U = 0$ in Figs. 4–6, hence their work

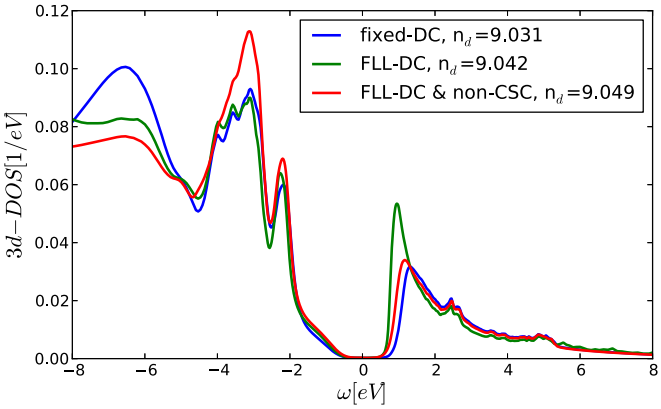

FIG. 10. (Color online) The $3d$ density of states within DFT+DMFT for La_2CuO_4 using the three different methodologies explained in Table I.

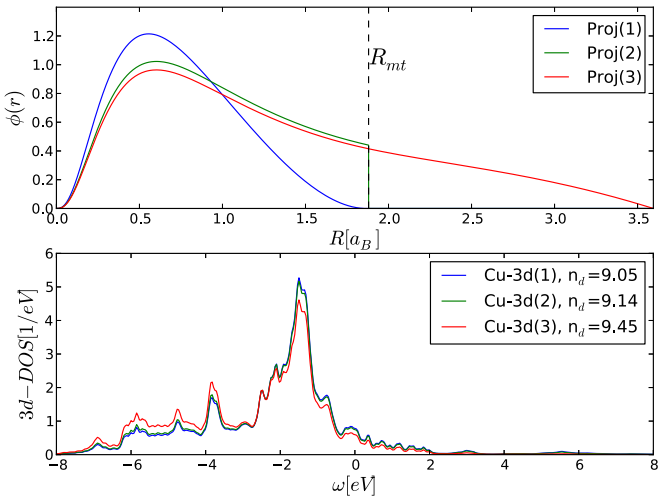

FIG. 11. (Color online) The radial dependence of the function $\phi(r)$, which defines the projector to the correlated $3d$ set of orbitals. Three different projectors [Proj(1), Proj(2), and Proj(3)] are defined in the upper panel. Lower panel shows the density of states within LDA for La_2CuO_4 using the three different projectors defined in the upper panel.

revealed difficulties with the formulation and implementation of DFT+DMFT when the Wannier basis is not sufficiently localized.

To understand the difference, we implemented a flexible real space projectors, which generalize atomiclike projectors introduced in Ref. [42], but can be extended into an interstitial region or made very localized inside an MT sphere. The form of such a projector in real space is

$$P(l,m,lm',\mathbf{rr}') = Y_{lm}(\hat{\mathbf{r}})\phi_l(r)\phi_l(r')Y_{lm'}(\hat{\mathbf{r}}'). \quad (2)$$

In the above calculations, the projector was constructed from $\phi_l(r)$, which is a solution of the Dirac equation inside the muffin-tin sphere, and is zero outside the sphere. In the actual implementation of Ref. [42], we also added the small contribution coming from the energy derivative of the radial wave function, which turns out not to be important in these cases. Here we allow $\phi_l(r)$ to be any radial wave function constructed from solution of the Dirac equation $u_l(r,E_\nu)$ with E_ν positioned at the center of the band, its first $[du_l(r,E_\nu)/dE_\nu \equiv \dot{u}_l]$ and second derivative $[d^2u_l(r,E_\nu)/d^2E_\nu = \ddot{u}_l]$. To gain an insight into the precise definition of the n_d occupancy, we projected the Kohn-Sham solution to the variety of projectors, spanning the range of very localized to moderately delocalized, using a linear combination of above defined functions: $\phi(r) = au_l(r) + b\dot{u}_l(r) + c\ddot{u}_l(r)$. First we choose a very localized function $\phi(r)$ entirely contained in the MT sphere and vanishing at the sphere with vanishing derivative. We name the corresponding projector Proj(1) in Fig. 11. (Here the MT spheres are chosen in such a way that the spheres of neighboring atoms touch.) Notice that such combination of u_l, $\dot{u}_l$, and $\ddot{u}_l$ roughly corresponds to choosing the linearization energy at the bottom of the corresponding bands.

The second projector Proj(2) takes u_l only (i.e., sets b and c to zero, hence linearization energy is taken at the middle of the corresponding band), but it truncates the radial function at the MT sphere. This projector is very similar to what is used in Sec. III of this paper. (The precise definition, which includes the correction due to $\dot{u}$ can be found in Ref. [42].) Finally, we extended the projector to the interstitial region with projector Proj(3). Inside the MT sphere we choose u_l as in Proj(2), and outside we choose linear combination of u_l, $\dot{u}_l$, and $\ddot{u}_l$ such that the function vanishes at the nearest neighbor oxygen, and is continuous differentiable across the MT sphere. When projecting the Kohn-Sham solution to the function $\phi(r)$ beyond the MT sphere of the $3d$ ion ($r > R_{\rm MT}$), we project to the plane-wave envelope functions only, to excluded the density concentrated inside the oxygen MT spheres, which should not be counted as transition metal charge. We always normalize the projector to exclude the trivial effect of volume increase.

TABLE II. The occupancy of the $3d$ orbitals using DFT (at $U = 0$) for the three projectors shown in Fig. 11. The MT spheres are listed in Table I.

n_d (DFT)	Proj(1)	Proj(2)	Proj(3)
La_2CuO_4	9.040	9.131	9.450
$LaVO_3$	2.096	2.193	2.872
$LaTiO_3$	1.097	1.195	1.960
$SrVO_3$	1.692	1.815	2.567

In Fig. 11 we show the radial functions $\phi(r)$ for these three projectors in the case of La_2CuO_4, together with the DFT projected density of states (more precisely $-\mathrm{Im}[G_d(\omega)]$). As is clear from the figure, the more delocalized projector has substantially more weight in the region between -7 and -4 eV, in the energy where oxygen is concentrated, while the localized projectors have more weight at the upper edge of the DOS and less concentrated around oxygen. The net result is a different occupancy n_d. In Table II we list the DFT occupancies obtained by projecting to these three projectors and for all compounds studied here. We again project to t_{2g} states for early transition metal oxides, and to e_g and t_{2g} states in La_2CuO_4, because these are the states which are correlated in the DMFT calculations. For La_2CuO_4 we notice that the two localized projectors [Proj(1) and Proj(2)] both have occupancy close to nominal d^9, and that the projector Proj(2) has slightly more charge (1% increase) than the most localized Proj(1). As shown by direct DFT+DMFT calculation above, Proj(2) gives the Mott insulating state in La_2CuO_4 irrespective of small details in double counting (fixed DC or FLL-DC) or charge self-consistency. On the other hand, Proj(3), which extends beyond the MT boundary, contains some of the charge that should have been assigned to other itinerant states. As a result, it gives occupancy $n_d = 9.45$, almost identical to the charge on the Wannier orbitals of Ref. [49]. Since construction of Wannier orbitals inevitably results in some fraction of electrons being delocalized beyond the MT boundary, it is not surprising that the $3d$ occupancy is similar to our more delocalized projector. Namely, maximally localized Wannier orbitals need to faithfully represent a set of low energy bands, hence their localization is constrained to this condition. We verified that DFT+DMFT solution using Proj(3) and FLL-DC results in metallic state, similar to finding of Ref. [49].

For the insulating early transition metal oxides, the t_{2g} occupancies of both localized projectors Proj(1) and Proj(2)

are again quite close to nominal valence, namely d^1 for $LaTiO_3$ and d^2 for $LaVO_3$. On the other hand, the delocalized projector Proj(3) results in much larger n_d, even larger than reported in Refs. [49,50]. Hence, Wannier orbitals in Ref. [50] are more localized than our Proj(3), but less than Proj(2) or Proj(1). We verified that decreasing localization of the projector always results in increased n_d occupancy. The Mott state within DFT+DMFT is again very robust using Proj(1) and Proj(2), but not when Proj(3) is used. Finally, the $3d$ occupancy in $SrVO_3$ is quite far from nominal d^1 valence even when using very localized projectors, and hence this mixed valency results in a metallic state even for very large values of local Coulomb repulsion U, in agreement with experimental observation of a metallic state in $SrVO_3$.

In the early transition metal oxides, we projected the Kohn-Sham solution to the t_{2g} states, because the center of the e_g states is sufficiently above the Fermi level that it does not require dynamic treatment within the DMFT. Since the e_g states strongly hybridize with the oxygen, the e_g occupancy does not exactly vanish. However, the DFT+DMFT solution is very sensitive to the correlated t_{2g} occupancy in early transition metal oxides, since the e_g states behave very differently, having a large gap. Hence, the e_g and t_{2g} charge should not be counted together when assessing stability of the DMFT insulating solution, hence we presented the t_{2g} charge only in Tables I and II.

V. CONCLUSIONS

We have shown in this paper that with the DFT+DMFT methodology of Ref. [42], a reasonable qualitative agreement between theory and experiment for the p and d spectra across the transition metal series is obtained, even when the Coulomb repulsion U and J are fixed across the entire series, hence no tuning parameter is needed for qualitative description of correlated solids, which is a requirement for any *ab initio* predictive method. This was possible because the DFT+DMFT method is implemented with a very localized projector, where the screening of the Coulomb repulsion by other valence states through hybridization is very efficient.

A large effort was undertaken recently by several groups [42–47] to implement DFT+DMFT in a way that does not require tuning parameters, and that has *ab inito* predictive power. In our opinion, such a mature state of DFT+DMFT has largely been reached, as demonstrated on early and late transition metal oxides here. This method gives a zeroth-order picture of the physics in correlated materials such as transition metal oxides. However, the position of oxygen states is not very precise in some compounds (see $LaTiO_3$), and better treatment of exchange would be needed to mitigate this deficiency. It was recently proposed in Ref. [90] that an additional Hartree term due to nonlocal interaction U_{pd} could mitigate this problem. However, in the charge self-consistent DFT+DMFT used here, the Hartree terms are taken into account exactly, and therefore no extra Hartree shifts are justified. Further corrections could come only from better treatment of the nonlocal exchange. Furthermore, the gap sizes of Mott insulators and positions of Hubbard bands can be improved by calculating Coulomb U more precisely from first principles. This is an important open problem in condensed matter theory. Methods such as GW [91] and constrained RPA [92] show some promise in this direction, but more work is needed to get precise enough values of U for modern DFT+DMFT codes, which use localized atomic orbitals in a large energy window.

In our implementation of DFT+DMFT, the position of oxygen states is not very far from its DFT value, and quite insensitive to the value of the correlation strength, in contrast to the finding of Refs. [49,50]. While the position of the oxygen states in DFT are not always in very good agreement with experiment, their small displacement does not lead to a major failure of DFT+DMFT. This shortcoming of LDA is known to occur in other materials (see, for example, Ref. [93]) and can be corrected by a better treatment of the nonlocal exchange as in hybrid DFT or GW, but not by DMFT.

We have also shown in this paper that in transition metal oxides the self-consistent value of the correlated electronic charge n_d of LDA+DMFT is closer to nominal valence than its LDA value. A similar finding was reported in Ref. [53] when studying the actinide series and its compounds. A systematic comparison with the x-ray data confirmed that the LDA+DMFT systematically improves the value of the correlated charge n_f relative to its LDA value.

Finally, the DMFT method is an orbitally dependent method, and the results depend on the choice of the correlated set of orbitals. The convergence of the results with respect to the number of orbitals is not possible at present, because the quantum mechanical problem becomes too expensive to solve. The quality of the results hence rest on the educated choice of the correlated orbital (the choice of the projector) which determines the set of states that are treated very precisely, by summing all local Feynman diagrams, and those that are treated by DFT. Since DMFT truncates interaction and correlations beyond a single site, a more localized orbital is clearly a better choice in this method. To recover similar results in a more delocalized basis, one would clearly need to go beyond single site approximation, which increases computational expense exponentially.

We have shown that in transition metal oxides, the $3d$ occupancies (n_d) on the transition metal ion are not very far from nominal valence when a sufficiently localized radial function is chosen for the projector. This is true even on the DFT level. We have also explicitly demonstrated that the choice of a more delocalized radial orbital leads to valences substantially larger than the nominal valence, which posses a problem for DMFT method, as noted in Refs. [49,50]. For such a choice of correlated states, the nonlocal correlations would likely need to be considered to recover similar results as in more localized case.

In conclusion, we successfully tested our implementation of the DFT+DMFT method in $3d$ transition metal series. The method predicts qualitative features, such as existence of a metallic or insulating state starting from first principles. It can be made fully automated, and hence high-throughput screening of correlated materials is an attractive avenue for future research.

ACKNOWLEDGMENTS

We thank A. Georges, C. H. Yee, H. Park, and A. J. Millis for stimulating discussion. K.H. and G.K. were supported by NSF DMR-1405303, and NSF DMR-1308141, respectively.

[1] H. Bethe, Ann. Phys. (Leipzig) **392**, 55 (1928).
[2] A. Sommerfeld, Z. Elektrochem. Angew. Phys. Chem. **34**, 426 (1928).
[3] F. Bloch, Z. Phys. **57**, 545 (1929).
[4] A. A. Abrikosov, L. P. Gor'kov, and I. Ye. Dzyaloshinskii, *Quantum Field Theoretical Methods in Statistical Physics*, 2nd ed. (Pergamon, Oxford, 1965).
[5] N. F. Mott, Proc. Phys. Soc. London **49**, 72 (1937)
[6] N. F. Mott, *Metal-Insulator Transitions*, 2nd ed. (Taylor and Francis, London, 1990).
[7] M. Imada, A. Fujimori, and Y. Tokura, Rev. Mod. Phys. **70**, 1039 (1998).
[8] D. N. Basov, R. D. Averitt, D. van der Marel M. Dressel, and K. Haule, Rev. Mod. Phys. **83**, 471 (2011).
[9] P. Hohenberg and W. Kohn, Phys. Rev. **136**, B864 (1964).
[10] A. Georges and G. Kotliar, Phys. Rev. B **45**, 6479 (1992).
[11] W. Metzner and D. Vollhardt, Phys. Rev. Lett. **62**, 324 (1989).
[12] A. Georges, G. Kotliar, W. Krauth, and M. J. Rozenberg, Rev. Mod. Phys. **68**, 13 (1996).
[13] G. Kotliar and D. Vollhardt, Phys. Today **57**, 53 (2004).
[14] X. Y. Zhang, M. J. Rozenberg, and G. Kotliar, Phys. Rev. Lett. **70**, 1666 (1993).
[15] M. J. Rozenberg, G. Kotliar, and X. Y. Zhang, Phys. Rev. B **49**, 10181 (1994).
[16] A. Georges and W. Krauth, Phys. Rev. Lett. **69**, 1240 (1992).
[17] M. J. Rozenberg, G. Kotliar, H. Kajueter, G. A. Thomas, D. H. Rapkine, J. M. Honig, and P. Metcalf, Phys. Rev. Lett. **75**, 105 (1995).
[18] P. Limelette, A. Georges, D. Jerome, P. Wzietek, P. Metcalf, and J. M. Honig, Science **302**, 89 (2003).
[19] P. Semon and A.-M. S. Tremblay, Phys. Rev. B **85**, 201101(R) (2012).
[20] V. I. Anisimov, A. I. Poteryaev, M. A. Korotin, A. O. Anokhin, and G. Kotliar, J. Phys.: Condens. Matter **9**, 7359 (1997); A. I. Lichtenstein and M. I. Katsnelson, Phys. Rev. B **57**, 6884 (1998).
[21] G. Kotliar, S. Y. Savrasov, K. Haue, V. S. Oudovenko, O. Parcollet, and C. A. Marianetti, Rev. Mod. Phys. **78**, 865 (2006).
[22] K. Held, Adv. Phys. **56**, 829 (2007).
[23] S. Savrasov, G. Kotliar, and E. Abrahams, Nature (London) **410**, 793 (2001).
[24] X. Dai, S. Y. Savrasov, G. Kotliar, A. Migliori, H. Ledbetter, and E. Abrahams, Science **300**, 953 (2003).
[25] J. H. Shim, K. Haule, and G. Kotliar, Science **2007**, 1615 (2007).
[26] M. B. Zolfl, I. A. Nekrasov, Th. Pruschke, V. I. Anisimov, and J. Keller, Phys. Rev. Lett. **87**, 276403 (2001).
[27] K. Held, A. K. McMahan, and R. T. Scalettar, Phys. Rev. Lett. **87**, 276404 (2001).
[28] E. R. Ylvisaker, J. Kunes, A. K. McMahan, and W. E. Pickett, Phys. Rev. Lett. **102**, 246401 (2009).
[29] B. Amadon, S. Biermann, A. Georges, and F. Aryasetiawan, Phys. Rev. Lett. **96**, 066402 (2006).
[30] E. Pavarini, S. Biermann, A. Poteryaev, A. I. Lichtenstein, A. Georges, and O. K. Andersen, Phys. Rev. Lett. **92**, 176403 (2004).
[31] E. Pavarini, A. Yamasaki, J. Nuss, and O. K. Andersen, New J. Phys. **7**, 188 (2005).
[32] M. De Raychaudhury, E. Pavarini, and O. K. Andersen, Phys. Rev. Lett. **99**, 126402 (2007).
[33] I. A. Nekrasov, G. Keller, D. E. Kondakov, A. V. Kozhevnikov, Th. Pruschke, K. Held, D. Vollhardt, and V. I. Anisimov, Phys. Rev. B **72**, 155106 (2005).
[34] K. Ohta, R. E. Cohen, K. Hirose, K. Haule, K. Shimizu, and Y. Ohishi, Phys. Rev. Lett. **108**, 026403 (2012).
[35] E. Gorelov, M. Karolak, T. O. Wehling, F. Lechermann, A. I. Lichtenstein, and E. Pavarini, Phys. Rev. Lett. **104**, 226401 (2010).
[36] J. Mravlje, M. Aichhorn, T. Miyake, K. Haule, G. Kotliar, and A. Georges, Phys. Rev. Lett. **106**, 096401 (2011).
[37] H. Zhang, K. Haule, and D. Vanderbilt, Phys. Rev. Lett. **111**, 246402 (2013).
[38] G. H. Wannier, Phys. Rev. **52**, 191 (1937).
[39] F. Aryasetiawan, M. Imada, A. Georges, G. Kotliar, S. Biermann, and A. I. Lichtenstein, Phys. Rev. B **70**, 195104 (2004).
[40] T. Miyake, F. Aryasetiawan, and M. Imada, Phys. Rev. B **80**, 155134 (2009).
[41] S. Y. Savrasov and G. Kotliar, Phys. Rev. B **69**, 245101 (2004).
[42] K. Haule, C.-H. Yee, and K. Kim, Phys. Rev. B **81**, 195107 (2010).
[43] B. Amadon, F. Lechermann, A. Georges, F. Jollet, T. O. Wehling, and A. I. Lichtenstein, Phys. Rev. B **77**, 205112 (2008).
[44] B. Amadon, J. Phys.: Condens. Matter **24**, 075604 (2012).
[45] F. Lechermann, A. Georges, A. Poteryaev, S. Biermann, M. Posternak, A. Yamasaki, and O. K. Andersen, Phys. Rev. B **74**, 125120 (2006).
[46] O. Granas, I. Di Marco, P. Thunstrom, L. Nordstrom, O. Eriksson, T. Bjorkman, and J. M. Wills, Comput. Mater. Sci. **55**, 295 (2012).
[47] M. Aichhorn, L. Pourovskii, and A. Georges, Phys. Rev. B **84**, 054529 (2011).
[48] N. Marzari, A. A. Mostofi, J. R. Yates, I. Souza, and D. Vanderbilt, Rev. Mod. Phys. **84**, 1419 (2012).
[49] X. Wang, M. J. Han, L. de Medici, H. Park, C. A. Marianetti, and A. J. Millis, Phys. Rev. B **86**, 195136 (2012).
[50] H. T. Dang, A. J. Millis, and C. A. Marianetti, Phys. Rev. B **89**, 161113(R) (2014).
[51] J. H. Shim, K. Haule, and G. Kotliar, Nature (London) **446**, 513 (2007).
[52] J. H. Shim, K. Haule, S. Savrasov, and G. Kotliar, Phys. Rev. Lett. **101**, 126403 (2008).
[53] J. H. Shim, K. Haule, and G. Kotliar, Eur. Phys. Lett. **85**, 17007 (2009).
[54] K. Haule and G. Kotliar, Nat. Phys. **5**, 796 (2009).
[55] C.-H. Yee, G. Kotliar, and K. Haule, Phys. Rev. B **81**, 035105 (2010).
[56] M. E. Pezzoli, K. Haule, and G. Kotliar, Phys. Rev. Lett. **106**, 016403 (2011).
[57] Q. Yin, A. Kutepov, K. Haule, G. Kotliar, S. Y. Savrasov, and W. E. Pickett, Phys. Rev. B **84**, 195111 (2011).
[58] J.-X. Zhu, P. H. Tobash, E. D. Bauer, F. Ronning, B. L. Scott, K. Haule, G. Kotliar, R. C. Albers, and J. M. Wills, Eur. Phys. Lett. **97**, 57001 (2012).
[59] X. Deng, K. Haule, and G. Kotliar, Phys. Rev. Lett. **111**, 176404 (2013).
[60] H. C. Choi, B. I. Min, J. H. Shim, K. Haule, and G. Kotliar, Phys. Rev. Lett. **108**, 016402 (2012).
[61] H. C. Choi, K. Haule, G. Kotliar, B. I. Min, and J. H. Shim, Phys. Rev. B **88**, 125111 (2013).

[62] M. K. Stewart, J. Liu, R. K. Smith, B. C. Chapler, C.-H. Yee, K. Haule, J. Chakhalian, and D. N. Basov, J. Appl. Phys. **110**, 033514 (2011).
[63] M. K. Stewart, C.-H. Yee, J. Liu, M. Kareev, R. K. Smith, B. C. Chapler, M. Varela, P. J. Ryan, K. Haule, J. Chakhalian, and D. N. Basov, Phys. Rev. B **83**, 075125 (2011).
[64] Z. P. Yin, K. Haule, and G. Kotliar, Nat. Phys. **7**, 294 (2011).
[65] Z. P. Yin, K. Haule, and G. Kotliar, Nat. Mater. **10**, 932 (2011).
[66] M. Liu, L. W. Harriger, H. Luo, M. Wang, R. A. Ewings, T. Guidi, H. Park, K. Haule, G. Kotliar, S. M. Hayden, and P. Dai, Nat. Phys. **8**, 376 (2012).
[67] G. Lee, H. S. Ji, Y. Kim, C. Kim, K. Haule, G. Kotliar, B. Lee, S. Khim, K. H. Kim, K. S. Kim, K. S. Kim, and J. H. Shim, Phys. Rev. Lett. **109**, 177001 (2012).
[68] J. M. Tomczak, K. Haule, and G. Kotliar, Proc. Natl. Acad. Sci. USA **109**, 3243 (2012).
[69] K. Haule, Phys. Rev. B **75**, 155113 (2007).
[70] P. Werner, A. Comanac, L. de Medici, M. Troyer, and A. J. Millis, Phys. Rev. Lett. **97**, 076405 (2006).
[71] V. I. Anisimov, F. Aryasetiawan, and A. I. Lichtenstein, J. Phys.: Condens. Matter **9**, 767 (1997).
[72] J. Lee and K. Haule, arXiv:1403.2474v1.
[73] P. Blaha, K. Schwarz, G. K. H. Madsen, K. Kvasnicka, and J. Luitz, in *Wien2K*, edited by K. Schwarz (Technische Universitat Wien, Austria, 2001).
[74] J. P. Perdew, K. Burke, and M. Ernzerhof, Phys. Rev. Lett. **77**, 3865 (1996).
[75] M. J. Rey, Ph. Dehaudt, J. C. Joubert, B. Lambert-Andron, M. Cyrot, and F. Cyrot-Lackmann, J. Solid State Chem. **86**, 101 (1990).
[76] P. Bordet, C. Chaillout, M. Marezio, Q. Huang, A. Santoro, S.-W. Cheong, H. Takagi, C. S. Oglesby, and B. Batlogg, J. Solid State Chem. **106**, 253 (1993).
[77] D. A. MacLean, H. H. Ng, and J. E. Greedan, J. Solid State Chem. **30**, 35 (1979).
[78] T. Kajitani, K. Hiraga, T. Sakurai, M. Hirabayashi, S. Hosoya, T. Fukuda, and K. Oh-Ishi, Physica C **171**, 491 (1990).
[79] M. Jarrell and J. E. Gubernatis, Phys. Rep. **269**, 133 (1996).
[80] K. Momma and F. Izumi, J. Appl. Crystallogr. **44**, 1272 (2011).
[81] K. Yoshimatsu, T. Okabe, H. Kumigashira, S. Okamoto, S. Aizaki, A. Fujimori, and M. Oshima, Phys. Rev. Lett. **104**, 147601 (2010).
[82] K. Maiti and D. D. Sarma, Phys. Rev. B **61**, 2525 (2000).
[83] T. Yoshida, A. Ino, T. Mizokawa, A. Fujimori, Y. Taguchi, T. Katsufuji, and Y. Tokura, Europhys. Lett. **59**, 258 (2002).
[84] T. Takahashi, F. Maeda, H. Katayama-Yoshida, Y. Okabe, and T. Suzuki, A. Fujimori, S. Hosoya, S. Shamoto, and M. Sato, Phys. Rev. B **37**, 9788 (1988).
[85] T. Yoshida, K. Tanaka, H. Yagi, A. Ino, H. Eisaki, A. Fujimori, and Z.-X. Shen, Phys. Rev. Lett. **95**, 146404 (2005).
[86] M. Takizawa, M. Minohara, H. Kumigashira, D. Toyota, M. Oshima, H. Wadati, T. Yoshida, A. Fujimori, M. Lippmaa, M. Kawasaki, H. Koinuma, G. Sordi, and M. Rozenberg, Phys. Rev. B **80**, 235104 (2009).
[87] P. M. Woodward, Acta Crystallogr. Sect. A. **53**, 44 (1997).
[88] M. Cwik, T. Lorenz, J. Baier, R. Muller, G. Andre, F. Bouree, F. Lichtenberg, A. Freimuth, R. Schmitz, E. Muller-Hartmann, and M. Braden, Phys. Rev. B **68**, 060401(R) (2003).
[89] G. Sordi, A. Amaricci, and M. J. Rozenberg, Phys. Rev. Lett. **99**, 196403 (2007).
[90] P. Hansmann, N. Parragh, A. Toschi, G. Sangiovanni, and K. Held, arXiv:1312.2757.
[91] A. Kutepov, K. Haule, S. Y. Savrasov, and G. Kotliar, Phys. Rev. B **82**, 045105 (2010).
[92] F. Aryasetiawan, M. Imada, A. Georges, G. Kotliar, S. Biermann, and A. I. Lichtenstein, Phys. Rev. B **70**, 195104 (2004).
[93] Z. P. Yin, A. Kutepov, and G. Kotliar, Phys. Rev. X **3**, 021011 (2013).